Molecular Therapy
Methods & Clinical Development
Original Article

# Systemic delivery of an AAV9 exon-skipping vector significantly improves or prevents features of Duchenne muscular dystrophy in the Dup2 mouse

Nicolas Wein,[1,2] Tatyana A. Vetter,[1] Adeline Vulin,[1,5] Tabatha R. Simmons,[1] Emma C. Frair,[1] Adrienne J. Bradley,[1] Liubov V. Gushchina,[1] Camila F. Almeida,[1] Nianyuan Huang,[1] Daniel Lesman,[1] Dhanarajan Rajakumar,[1] Robert B. Weiss,[3] and Kevin M. Flanigan[1,2,4]

[1]Center for Gene Therapy, The Abigail Wexner Research Institute, Nationwide Children's Hospital, 700 Children's Drive, Columbus, OH 43205, USA; [2]Department of Pediatrics, The Ohio State University, Columbus, OH, USA; [3]Department of Human Genetics, The University of Utah School of Medicine, Salt Lake City, UT, USA; [4]Department of Neurology, The Ohio State University, Columbus, OH, USA

**Duchenne muscular dystrophy (DMD) is typically caused by mutations that disrupt the *DMD* reading frame, but nonsense mutations in the 5′ part of the gene induce utilization of an internal ribosomal entry site (IRES) in exon 5, driving expression of a highly functional N-truncated dystrophin. We have developed an AAV9 vector expressing U7 small nuclear RNAs targeting *DMD* exon 2 and have tested it in a mouse containing a duplication of exon 2, in which skipping of both exon 2 copies induces IRES-driven expression, and skipping of one copy leads to wild-type dystrophin expression. One-time intravascular injection either at postnatal days 0–1 or at 2 months results in efficient exon skipping and dystrophin expression, and significant protection from functional and pathologic deficits. Immunofluorescence quantification showed 33%–53% average dystrophin intensity and 55%–79% average dystrophin-positive fibers in mice treated in adulthood, with partial amelioration of DMD pathology and correction of DMD-associated alterations in gene expression. In mice treated neonatally, dystrophin immunofluorescence reached 49%–85% of normal intensity and 76%–99% dystrophin-positive fibers, with near-complete correction of dystrophic pathology, and these beneficial effects persisted for at least 6 months. Our results demonstrate the robustness, durability, and safety of exon 2 skipping using scAAV9.U7snRNA.ACCA, supporting its clinical use.**

## INTRODUCTION

Duchenne muscular dystrophy (DMD) is an X-linked degenerative muscle disorder that affects around 1 in 5,200 male births.[1] Symptoms of generalized muscle weakness first appear at age 3–5 years and progress to a loss of ambulation by age 13, with death typically occurring in the third decade of life due to cardiomyopathy or respiratory insufficiency.[2,3] DMD is caused by mutations that disrupt the open reading frame in the *DMD* gene, which encodes dystrophin,[4] a large (427 kDa) multifunctional protein that is localized at the subsarcolemmal region of myofibers, where it plays an important role in protecting the sarcolemma from mechanical damage caused by muscle contraction.[5] The presence of a partially functional dystrophin protein occurs with mutations that maintain an open reading frame, often resulting in the milder allelic disorder Becker muscular dystrophy (BMD).[6,7] Because of the variety of in-frame mutations resulting in a variety of partially functional proteins, BMD has a broad phenotypic spectrum with, for example, loss of ambulation ranging from the late teenage years to late adulthood.

Promising therapeutic approaches to DMD are based on the replacement of a functional version of *DMD* or its repair at the DNA or pre-mRNA level. Both approaches aim to restore an open reading frame, leading to expression of a partially functional, BMD-like dystrophin. Gene replacement trials are under way using modified adeno-associated viruses (AAVs)[8–10] but transgene packaging capacity of AAV is limited to ~5 kb. Because the *DMD* cDNA is 11.4 kb, some current gene therapy strategies rely on delivery of one of several engineered microdystrophin cDNAs, which carry internal deletions of the central rod domain and deletions of some of the C-terminal portion of the protein.[11,12] An alternative approach is to restore the mRNA reading frame by delivering an antisense sequence that binds to key exon definition elements in the pre-mRNA, inhibiting the recognition of a

Received 26 March 2022; accepted 8 July 2022;
https://doi.org/10.1016/j.omtm.2022.07.005.

[5]Present address: U1179 INSERM, UFR des Sciences de la Santé-LIA BAHN CSM, Université de Versailles St-Quentin, Montigny le Bretonneux, France

**Correspondence:** Nicolas Wein, PhD, The Center for Gene Therapy, The Research Institute, Nationwide Children's Hospital, The Ohio State University, 700 Children's Drive, Columbus, OH 43205, USA.
**E-mail:** nicolas.wein@nationwidechildrens.org
**Correspondence:** Kevin M. Flanigan, MD, The Center for Gene Therapy, The Research Institute, Nationwide Children's Hospital, The Ohio State University, 700 Children's Drive, Columbus, OH 43205, USA.
**E-mail:** kevin.flanigan@nationwidechildrens.org

specific exon by the spliceosome and leading to exclusion of the target exon from the mature RNA. Such antisense sequences can consist of antisense oligonucleotides (AONs), or phosphorodiamidate morpholino oligomers (PMOs) such as eteplirsen, the first such therapy approved by the US Food and Drug Administration (FDA) for the treatment of DMD caused by mutations amenable to skipping of exon 51.[13–15]

An alternative to the use of AONs, whose short half-life outside muscle fibers necessitates frequent reinjections, is to embed antisense targeting sequences into a modified U7 small nuclear RNA (U7snRNA).[16] This becomes a part of a small nuclear ribosomal protein complex (snRNP) that protects the antisense sequence from degradation and allows for accumulation in the nucleus where splicing occurs.[17] The U7snRNA, which contains internal promoters allowing for continuous transcription of the downstream antisense sequences, can be encapsidated into an AAV for widespread tissue delivery. This approach has been shown to be efficient *in vitro* as well as in mouse and dog models of DMD.[6,18–21]

Duplications of one or more exons cause up to 11% of all DMD cases, and duplications of exon 2 are the most common, accounting for 10% of all duplications.[22,23] Our group sought to test the U7snRNA approach to induce skipping of *Dmd* exon 2, with a particular goal of restoring wild-type (WT) dystrophin rather than an internally deleted BMD-like dystrophin. Targeting of exon 2 duplication mutations by exon skipping provides a very wide therapeutic window because of the highly beneficial nature of both potential skipped transcripts. Whereas skipping of a single copy of exon 2 results in a full-length WT dystrophin, skipping of both copies results in alternative translational initiation from a highly functional internal ribosome entry site (IRES) within exon 5.[14] Despite lacking the first calponin homology 1 (CH1) domain within N-terminal actin binding domain 1 (ABD1), the resulting protein is highly functional—as proven by the exceedingly mild phenotype in families who express this version of the protein due to a founder allele nonsense mutation within exon 1, many of whom have only myalgia and elevations in creatine kinase, and walk into their seventh decade or longer.[24]

The vector we developed contains four copies of the U7snRNA in a self-complementary genome, with two copies targeting the splice acceptor site (sequence A) and two targeting the splice donor site (sequence C), encapsidated in AAV9 (scAAV9.U7.ACCA). After demonstrating the efficacy of intramuscular and systemic delivery of this vector in the Dup2 mouse (which carries the analogous mutation),[25] we confirmed the induction of widespread dystrophin expression throughout the muscles and heart up to 3 months after treatment[26] without evidence of off-target splice alteration in mice[27] or of toxicity in non-human primates.[28] Here we investigate the efficacy of exon 2 skipping induced by this vector following systemic delivery with or without co-treatment with prednisolone, as steroids are the only treatment shown to slow progression of DMD and we have previously shown that the *DMD* IRES is glucocorticoid responsive.[14] We also explore the longevity of exon skipping and dystrophin restoration over the span of 6 months following neonatal treatment with scAAV9.U7.ACCA and document the amelioration of signs of DMD pathology in treated Dup2 mice.

One-time tail vein injection of scAAV9.U7.ACCA into 2-month-old Dup2 mice resulted in highly efficient exon skipping, translation of both full-length and IRES-driven dystrophin proteins, and correction of histopathological and functional markers of disease. Similarly, a single neonatal injection of this vector resulted in highly efficient and sustained exon skipping, dystrophin production, and almost complete correction of the disease phenotype at 6 months. Importantly, treatment of Dup2 mice with scAAV9.U7.ACCA fully or partially corrected the expression of many genes that have been documented to be differentially expressed in dystrophic versus healthy muscle. Together, our results support a promising therapeutic option for patients with exon 2 duplications and strengthen the rationale for further development of this therapy, which has already reached its first-in-human clinical trial (NCT04240314).

## RESULTS

### Systemic delivery of scAAV9.U7.ACCA mediates efficient exon 2 skipping and dystrophin restoration in muscles of Dup2 adult mice

To determine whether systemic delivery of scAAV9.U7.ACCA (ACCA) mediates efficient exon skipping and dystrophin expression, 2-month-old Dup2 mice received tail vein injections of the vector at $7.6 \times 10^{13}$ vector genomes per kilogram body weight (vg/kg). Because the activity of the exon 5 IRES is increased in the presence of a glucocorticoid (6α-methylprednisolone 21-hemisuccinate sodium salt [PDN]), two additional groups of PDN-treated mice were also included (PDN alone and ACCA + PDN). Three months later, quantitative PCR (qPCR) was used to assess vector biodistribution, showing a range of 2.8–17.5 vg/dg across different tissues and both ACCA treatment groups (Figure S1 and Table S1). Although two-way ANOVA found a significant treatment effect between ACCA and ACCA + PDN ($p = 0.009$), with ACCA + PDN trending toward higher biodistribution in all tissues except the heart, the multiple comparisons for each individual tissue did not reach the level of significance (Table S1).

Efficient exon 2 skipping was confirmed by RT-PCR on RNA from individual muscles and the heart, based on quantification of bands representing two copies (Dup2), one copy (WT), or no copies (Del2) of exon 2 (Figures 1A and S2). Both WT and Del2 transcripts are therapeutic, since they result in translation of either the WT or IRES-driven dystrophin isoforms, respectively. Overall, 69%–95% of the mRNA in the ACCA and ACCA + PDN groups consisted of therapeutic, skipped transcripts (Figure 1B and Table S2). No significant difference in exon 2 skipping was found between the ACCA and ACCA + PDN groups in any of the tissues.

Western blots were performed to quantify the degree of dystrophin restoration relative to a standard curve of pooled WT C57Bl6 (Bl6) tissue (Figures 1C and S3). The two ACCA-treated groups showed

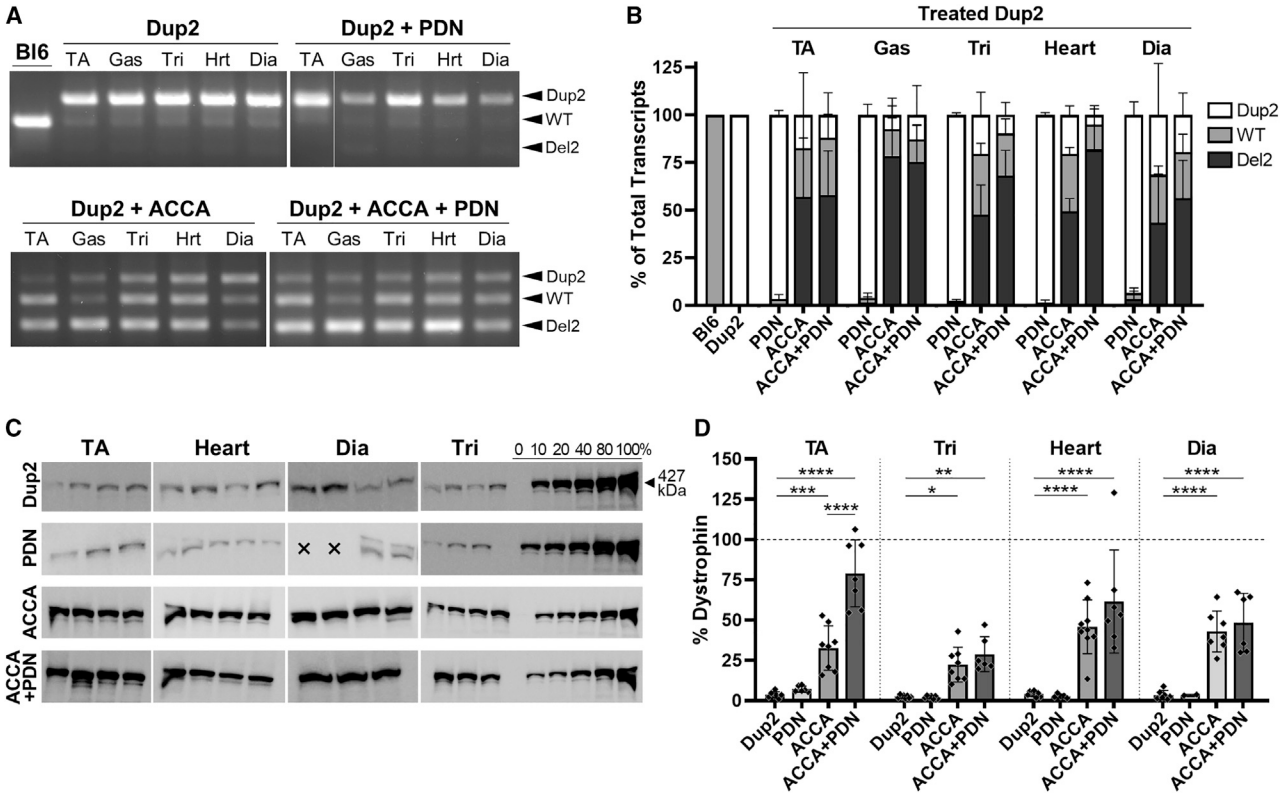


**Figure 1. Systemic delivery of scAAV9.U7.ACCA in adult Dup2 mice results in robust skipping of *Dmd* exon 2 and induction of dystrophin expression**

(A) Representative RT-PCR gel images of tibialis anterior (TA), gastrocnemius (Gas), triceps (Tri), heart, and diaphragm (Dia) RNA from Dup2 mice treated with $7.6 \times 10^{13}$ vg/kg scAAV9.U7.ACCA (ACCA), methylprednisolone (PDN), or both agents 3 months post injection, compared with untreated Dup2 and wild-type (WT) (Bl6) control mice. Primers for *Dmd* exon 1 and exon 3 produce three amplicons containing either two copies (Dup2, 340 bp), one copy (WT, 278 bp), or no copies (Del2, 216 bp) of exon 2. (B) Quantification of RT-PCR amplicon bands shown in (A), presented as mean ± SD (n = 4–6 per group). (C) Representative western blots of TA, Dia, Heart, and Tri dystrophin levels in Dup2 mice treated with scAAV9.U7.ACCA (ACCA), methylprednisolone (PDN), or both agents 3 months post injection compared with untreated Dup2 mice. The quantification standard curve on the right shows incremental dilutions of pooled Bl6 samples in dystrophin-null muscle lysate. Crosses indicate empty lanes. (D) Quantification of western blot bands shown in (C). The dashed line indicates 100% based on the Bl6 standard curve. Data are presented as mean ± SD with individual points. Statistical comparisons were performed using two-way ANOVA with Sidak multiple comparisons test. *$p < 0.05$; **$p < 0.01$; ***$p < 0.001$; ****$p < 0.0001$.

effective restoration of protein expression, with a pattern of somewhat higher mean dystrophin expression in the ACCA + PDN group that was not significantly different from the ACCA group in any tissues except the tibialis anterior (TA) (Figure 1D and Table S3). The lowest levels of ACCA-mediated dystrophin restoration by western blot were found in the triceps at 22.4% and 28.9% without and with PDN, respectively. In the heart and the TA, mean dystrophin levels in mice treated with ACCA + PDN reached 61.6% and 79.1%, respectively, with some samples approaching or exceeding 100% based on the standard curve (Figure 1D).

Immunofluorescence analysis using a C-terminal antibody that recognizes both IRES-driven and full-length dystrophin confirmed that ACCA treatment with or without PDN resulted in widespread restoration of dystrophin to the sarcolemma (Figures 2A and S4). Automated unbiased quantification of muscle immunofluorescence[26,29] showed a range of 32.8%–45.7% dystrophin intensity (Figure 2B and Table S3) and 54.9%–79.1% dystrophin-positive fibers (PDPF) (Figures 2C and S4; Table S3) on average in different muscles, with several individual samples from both ACCA treatment groups having PDPF above 90%. Although automated PDPF measurements were not possible in the heart at the available image resolution, mean cardiac dystrophin intensity was the highest of all tissues at 47.4%–53.3% of Bl6 with and without PDN, respectively (Figures 2B and S5; Table S3). Immunofluorescence analysis did not reveal any significant differences between ACCA treatment groups with and without PDN. In all protein assays, PDN alone had no significant effect on dystrophin expression in the absence of ACCA.

### Rescue of the dystrophin-glycoprotein complex and reduction of muscle pathology after systemic delivery of scAAV9.U7.ACCA in Dup2 adult mice

One of the primary roles of dystrophin is to link the cytoskeleton to the extracellular matrix via the dystrophin-glycoprotein complex (DGC). In the absence of dystrophin, this complex is disrupted or mislocalized, and recovery of the complex would be

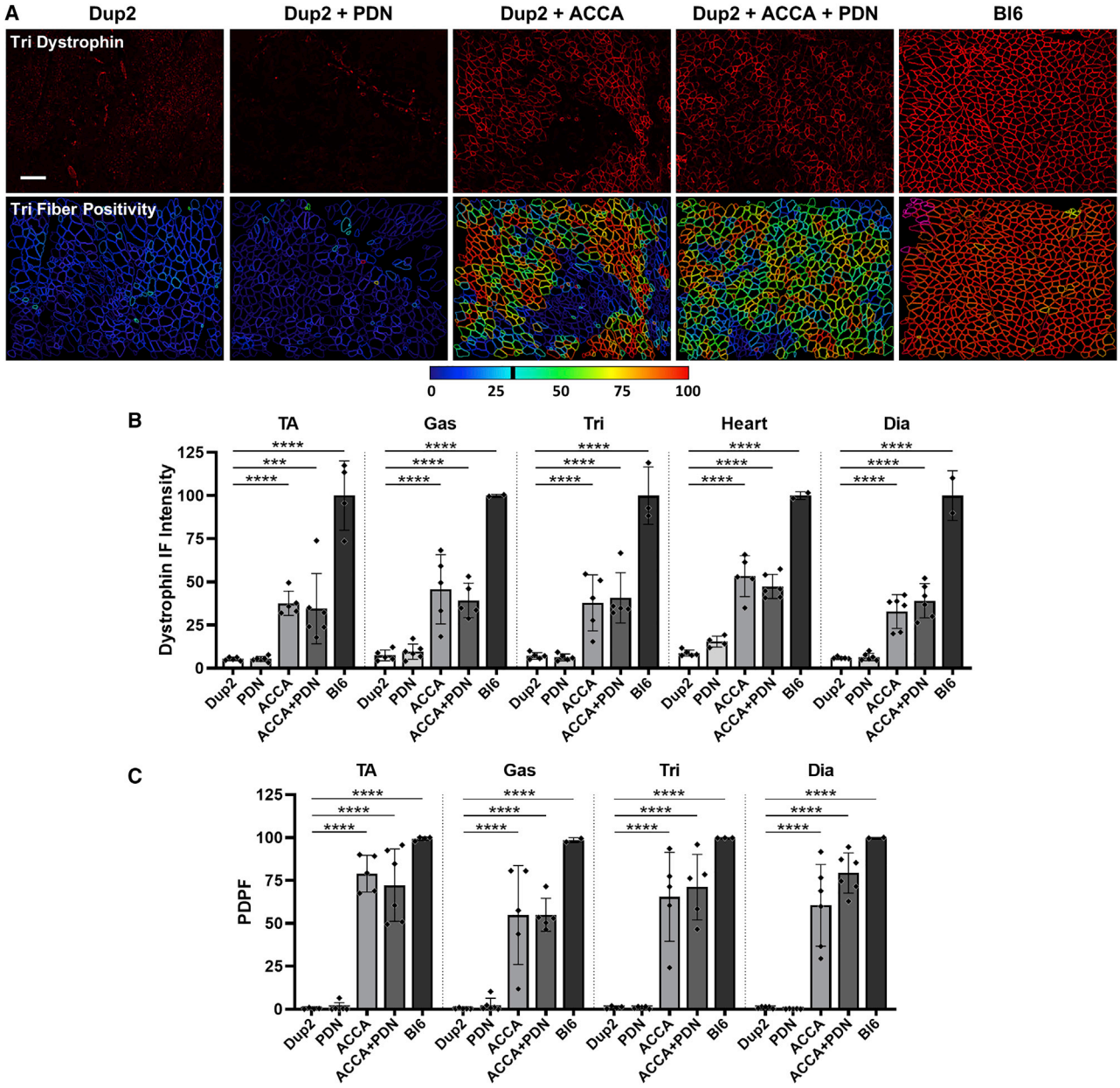


**Figure 2. Adult Dup2 mice show widespread sarcolemmal dystrophin restoration following treatment with scAAV9.U7.ACCA**

(A) Representative images of dystrophin immunofluorescence in Tri sections confirm proper dystrophin localization (red) and reflect quantification of fiber dystrophin positivity. Images were processed identically with shading correction, rolling-ball background subtraction, and denoising (see Figure S4 for unprocessed images). Color-coded heatmaps reflect the percent dystrophin-positive perimeter for each muscle fiber, as indicated by the color scale. Fibers that have dystrophin around ≥30% of the perimeter are considered dystrophin positive. Scale bar, 200 μm. (B and C) Quantification of dystrophin immunofluorescence (IF) intensity (B) and percent dystrophin-positive fibers (PDPF) (C) in muscle and heart sections. All data are presented as mean ± SD with individual points. All statistical comparisons were performed using two-way ANOVA with Sidak multiple comparisons test. ***$p < 0.001$; ****$p < 0.0001$.

expected from therapeutic dystrophin restoration. We evaluated sarcolemmal expression of the DGC proteins β-sarcoglycan (β-SG) and β-dystroglycan (β-DG), and of neuronal nitric oxide synthase (nNOS), a protein that binds to dystrophin to localize to the subsarcolemmal region where it plays a role in signal transduction pathways implicated in DMD pathogenesis.[30] Treatment with ACCA or ACCA + PDN resulted in widespread recovery of β-SG, β-DG, and nNOS in all tested muscles, whereas PDN alone did not show a meaningful effect compared with untreated muscle (Figures 3A and S6).

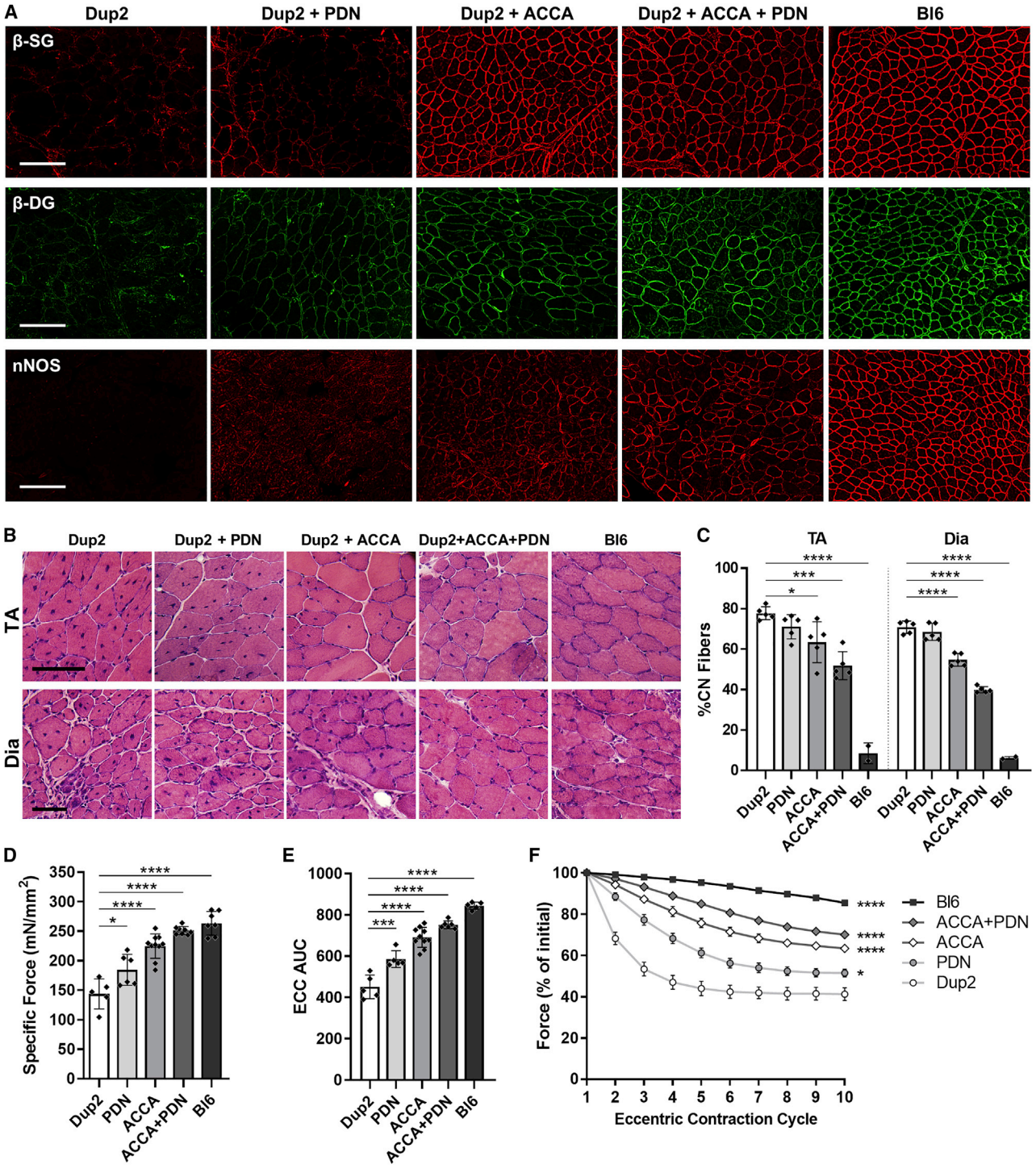


**Figure 3. Restoration of dystrophin by scAAV9.U7.ACCA in adult Dup2 mice enhances sarcolemmal localization of dystrophin binding partners and ameliorates muscle pathology**

(A) Immunostaining of β-sarcoglycan (β-SG), β-dystroglycan (β-DG), and neuronal nitric oxidase synthase (nNOS) in tibialis anterior of Dup2 mice treated with scAAV9.U7.ACCA (ACCA), methylprednisolone (PDN), or both agents 3 months post injection compared with age-matched control mice. Scale bars, 200 μm. Images represent n = 5–6 per group. (B) Representative H&E staining of tibialis anterior (TA) and diaphragm (Dia) from treated Dup2 and control mice. Scale bars, 100 μm. (C) Quantification of centronucleation (CN) in myofibers from TA and diaphragm H&E images. (D) TA specific force measured during tetanic contraction. (E) Magnitude of TA force drop over ten

*(legend continued on next page)*

Histopathological assessment of TA and diaphragm sections stained with hematoxylin and eosin (H&E) showed signs of reduced myofiber necrosis and central nucleation with ACCA treatment compared with untreated and PDN-treated Dup2 controls (Figures 3B and 3C). Central nucleation decreased from 77.8% in untreated Dup2 to 51.9% with ACCA + PDN in the TA, and from 70.9% to 39.9% in the same groups in the diaphragm. Furthermore, the combined treatment group showed a significantly greater reduction in central nucleation in the diaphragm compared with ACCA alone ($p < 0.0001$), but the same comparison was not statistically significant in the TA (Figure 3C). Central nucleation in all untreated and treated Dup2 groups was significantly different from Bl6 ($p < 0.0001$ for all comparisons; not marked on graph).

*In vivo* muscle function assessments confirmed that treatment with ACCA or ACCA + PDN resulted in significant improvements in force generation and amelioration of eccentric contraction-induced functional deficits. TA muscles from untreated Dup2 mice exhibited a 45% reduction in specific force compared with Bl6 muscle (144 mN/mm$^2$ versus 264 mN/mm$^2$) (Figure 3D), which was corrected to near-WT levels by ACCA treatment, with modestly stronger correction after combined treatment with ACCA + PDN (Figure 3D and Table S4). A hallmark exaggerated force drop was also observed in untreated Dup2 TA muscle over ten repeated cycles of eccentric contractions (ECC), which was partially corrected in all treatment groups, with the strongest correction in the combined ACCA + PDN group. The area under the curve (AUC) of the ECC tracings was reduced to 53.4% of Bl6 in untreated Dup2 mice, and was restored to 81.8% of Bl6 with ACCA treatment and 89.1% with ACCA + PDN (Figure 3E and Table S4). At the final ECC, the average degree of force loss was 14.5% in Bl6 versus 58.7% in untreated Dup2, and was partially corrected by ACCA alone (36.6% force loss) and ACCA + PDN (29.8% force loss) (Figure 3F and Table S4). Interestingly, all measures of muscle function also showed a small but significant benefit from treatment with PDN alone compared with untreated Dup2. Together, these results confirm that the dystrophin isoforms induced by systemic delivery of ACCA in adult Dup2 mice are highly functional and protective.

### Correction of gene expression abnormalities after systemic delivery of scAAV9.U7.ACCA in Dup2 adult mice

RNA from TA specimens was analyzed by ribosome profiling analysis (RPF) (Figure 4A), which allows inferences regarding the translational activity of the mRNA by mapping the distribution of ribosome-protected mRNA fragments onto the *DMD* transcript. We found that the cumulative distribution of *Dmd* RPF reads covered most of the *Dmd* transcript in the untreated sample. Although the source of this coverage is unknown, it is consistent with a model that would have the translation initiation near the 5′ end of the mRNA. Interestingly, there is an inflection point of coverage near the beginning of the Dp71 isoform. In the untreated samples, more than 30% of the total RPF coverage is generated from the Dp71 region. In contrast, the treated sample demonstrated less than 15% of the total RPF coverage mapped to the Dp71 region and had a more uniform coverage across the length of the transcript, consistent with increased translation from the 5′ end of the mRNA.

To determine whether the treatment corrects the transcriptome of the Dup2 muscle, we evaluated expression of a group of genes that are dysregulated in DMD patients.[31] RNA-sequencing (RNA-seq) data (Table S5) indicated that treatment restored a "non-dystrophic" gene expression profile by reversing the direction and magnitude of differentially expressed genes previously identified in dystrophic skeletal muscle from DMD patients. Genome-wide normalized RPF-sequencing (RPF-seq) data also showed that untreated Dup2 TA samples have a dystrophic transcriptional profile, whereas treatment results in a general correction in the level of expression. Levels of previously downregulated genes were increased and those of upregulated genes decreased (Figure 4B and Table S5), consistent with a general correction in the global expression pattern. In addition, the *Dmd* transcript showed clearly increased RPF reads in the treated sample, indicating that the treatment specifically increased dystrophin translation.

### Early systemic delivery of scAAV9.U7.ACCA in neonatal Dup2 mice drives persistent exon skipping and dystrophin expression

To determine whether earlier treatment could prevent muscle degeneration, neonatal mice were treated with a single systemic infusion of scAAV9.U7.ACCA at 0–1 postnatal days of age (P0–P1) using a higher dose of $3.2 \times 10^{14}$ vg/kg, and were sacrificed at 1, 3, and 6 months post injection. Vector biodistribution showed 4.7–25.0 vg/dg in muscles and 87.7–95.3 vg/dg in the heart by qPCR, and vector genome levels remained roughly stable between the 3- and 6-month time points (Figure S1 and Table S1). *Dmd* transcripts were evaluated by RT-PCR, again demonstrating highly efficient exon skipping across all tissues (Figure 5A and Table S6). Importantly, despite a slight decrease in skipping efficiency at the 3-month time point, the proportion of therapeutic transcripts measured at 6 months (89.3%–97.6% of total) was similar to levels seen at 1 month (82.8%–92.7%) (Figure 5A and Table S6), providing evidence of a robust and sustained effect following a single ACCA injection.

Western blots corroborated this persistent restoration of protein expression in the triceps, with 38.0% dystrophin relative to the Bl6 standard curve at 3 months and 28.7% at 6 months (Figures 5B and 5C; Table S7), although the difference is not significant owing to high intragroup variability and considerable overlap between the groups.

cycles of eccentric contractions (ECC), reflecting the area under the curve (AUC) of the ECC force tracings. (F) ECC-induced force loss tracings for the TA reflecting ten eccentric contraction cycles. All bar graph data are presented as mean ± SD with individual points, and statistical comparisons were performed using one-way ANOVA with Sidak multiple comparisons test. ECC cycle tracings show mean ± SEM and were compared using two-way ANOVA with Bonferroni multiple comparisons test. *$p < 0.05$; ***$p < 0.001$; ****$p < 0.0001$ versus Dup2.

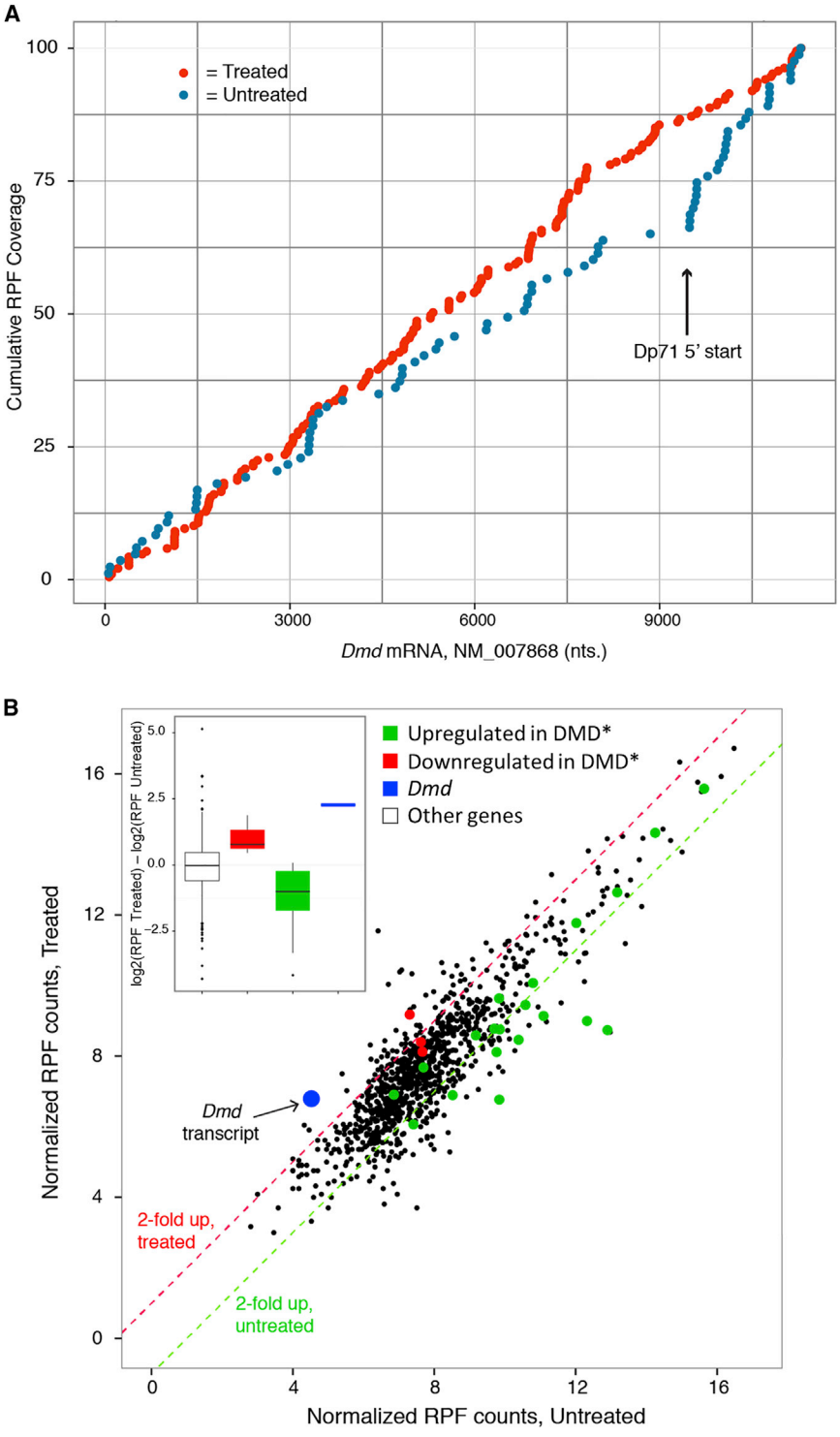


**Figure 4. Correction of *Dmd* and genome-wide gene expression profiles in adult Dup2 mice following treatment with scAAV9.U7.ACCA**

(A) Cumulative ribosome-protected fragment (RPF) coverage from scAAV9.U7.ACCA treated (red) and untreated (blue) mouse Dup2 tibialis anterior (TA) muscle. The arrow indicates the location of the 5′ end of the Dp71 transcript. (B) Dup2 mouse genome-wide levels of RPF-seq reads from scAAV9.U7.ACCA-treated versus untreated TA muscle, confirming correction of genes differentially expressed in DMD muscle. *List of genes upregulated and downregulated in DMD muscle is based on Haslett et al.[31]

Immunofluorescence confirmed appropriate localization and widespread restoration of dystrophin in the muscles and heart (Figures 5D and S8–S10), with mean dystrophin signal intensities ranging from 48.7% to 85.2% of mean Bl6 intensity (Figure 5E and Table S5) and PDPF ranging from 76.4% to 98.6% (Figures 5F and S9; Table S7) in ACCA-treated mice. Many individual samples displayed WT-like dystrophin expression, particularly in the diaphragm, which had the highest dystrophin intensity and PDPF at both post-treatment time points (Figure 5E). Immunofluorescence data did not show any evidence of a consistent change in dystrophin expression over time, and no significant time-point effect was found using two-way ANOVA. Overall, mice treated with ACCA neonatally at the higher dose showed a trend toward stronger dystrophin restoration at the sarcolemma compared with mice treated at 2 months of age. When plotted according to dystrophin immunofluorescence intensity versus PDPF, 75% of the tissue samples from Dup2 mice treated neonatally occupy the high-intensity-high-PDPF quadrant (above 50% for both parameters) and 23% fall into the low-intensity-high-PDPF quadrant. In contrast, 19% of the samples from mice treated in adulthood fall into the high-intensity-high-PDPF quadrant, 58% fall into the low-intensity-high-PDPF quadrant, and the remaining 23% land in the low-intensity-low-PDPF quadrant (Figure S11).

### Early systemic delivery of scAAV9.U7.ACCA in neonatal Dup2 mice corrects muscle structure and function without any significant off-target pathology

Muscle function testing revealed that tetanic specific force markedly improved at 3 months and 6 months after neonatal ACCA treatment, reaching 76.7%–87.9% of Bl6 muscle versus 51.1%–51.5% in untreated Dup2 (Figures 6A and 6B; Table S8). ECC-induced force loss was corrected to near-WT levels at both post-treatment time points, reflected by mean ECC AUC values of 93.7% of Bl6 at 3 months and 96.2% at 6 months in the treated

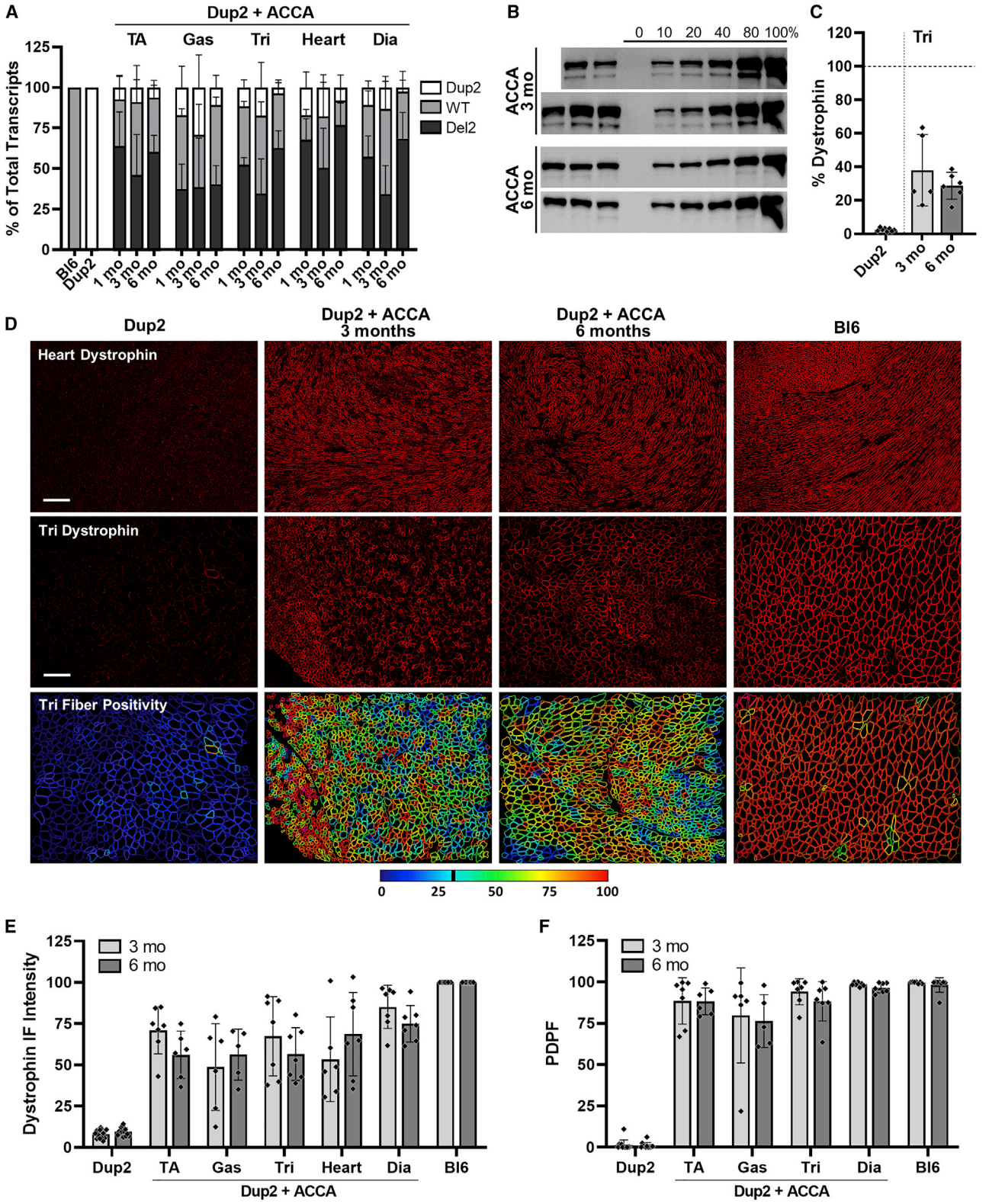


*(legend on next page)*

Dup2 (Figures 6A and 6B; Table S8). Functional correction appeared more complete at the 6-month time point, where mean force loss at the final ECC in ACCA-treated Dup2 mice was not statistically different from that in Bl6 mice, further providing evidence of the longevity of the treatment (Figures 6C and 6D; Table S8).

Muscle sections from ACCA-treated animals appeared histologically normal with no significant signs of necrosis or immune cell infiltration, and treated muscle revealed almost no central nucleation, indicating that the early treatment prevented muscle degeneration for at least 6 months (Figures 6E and 6F). Histopathologic analysis was performed on various non-muscle organs by a trained pathologist, who reported occasional patchy small foci of inflammation that may contain neutrophils in several livers, but no signs of pathology in other tissues up to 6 months after injection (Figure S12).

## DISCUSSION

Our results confirm those of our previous studies of exon 2 skipping in cell culture as well as in mice following intramuscular or systemic injection, the latter of which showed that systemic delivery of scAAV9.U7.ACCA drives highly efficient production of therapeutic WT and Del2 *Dmd* transcripts that are translated into either full-length dystrophin or the highly functional IRES-driven dystrophin isoform.[14,26] Extending our previous results, here we demonstrate that a one-time systemic injection of scAAV9.U7.ACCA in adult Dup2 mice restores sarcolemmal expression of dystrophin binding partners, ameliorates muscle pathology, and corrects gene expression changes observed in dystrophic muscle. We further demonstrate that a single systemic injection of scAAV9.U7.ACCA in neonatal mice led to sustained exon skipping and dystrophin restoration for at least 6 months and markedly decreased histological and functional pathological features in the Dup2 mouse over the same time period, consistent with the high degree of exon skipping efficiency.

Such vectorized exon skipping holds significant promise for overcoming limitations of other exon-skipping approaches used in DMD. Currently there are four FDA-approved exon-skipping therapies for DMD using antisense PMOs. Although promising, current PMO therapies require weekly reinjections; furthermore, they have shown only low-level correction of dystrophin expression in skeletal muscle,[32–34] and in animal models they have shown limited efficacy in the heart.[35,36] In contrast, AAV-delivered U7snRNA-mediated exon skipping offers the advantage of robust targeting of all muscles including heart and diaphragm, and continuous antisense sequence transcription and accumulation in the nucleus (where splicing occurs) after a single injection. In the golden retriever muscular dystrophy (GRMD) dog model, which contains a point mutation that leads to exon 7 skipping and out-of-frame transcript, injection of an AAV.U7 vector targeting exons 6 and 8 results in efficient restoration of the reading frame and significant expression of dystrophin with long-lasting improvements in muscle function.[20,37] The safety of this approach is supported by our own studies with the scAAV9.U7.ACCA vector showing lack of significant toxicity in non-human primates[28] and the lack of off-target splicing alteration in the Dup2 mouse model at clinically relevant doses.[27] In contrast to a study from another group using a vector targeting a different exon that demonstrated loss of AAV.U7 genomes and reduction of dystrophin expression over time,[38] we did not observe any reduction of skipping efficiency or protein expression over the length of our study. This may reflect differing efficiency due to the injection time point used, differences in the underlying efficacy of our vector, or differences in response between the different mouse models studied.

Treatment with scAAV9.U7.ACCA consistently resulted in robust dystrophin expression as assessed by both immunofluorescence and western blot quantification at levels that would be expected to have a significant impact on disease severity. In these treated Dup2 mice, levels of dystrophin as measured by western blot reached an average of at least 22% of normal; in comparison, values of 5%–20% have been associated with BMD,[39] and dystrophin levels as low as 3.2% of normal can significantly ameliorate disease symptoms in dystrophinopathy patients.[40] The observed levels are greater than those seen in patients with the c.9G>A founder allele who express the IRES-driven dystrophin isoform at levels of 5%–15% of normal, allowing ambulation into the seventh or eighth decade.[24] Inducing expression of these full-length and/or IRES-driven dystrophins resulted in significant improvements of muscle function compared with untreated mice. Notably, the muscle with the greatest degree of dystrophin restoration in Dup2 treated neonatally—with values of nearly 100% of WT—was the diaphragm, the degeneration of which results in respiratory failure, the most common cause of death in DMD. Co-treatment with PDN resulted in statistically significant improvement in TA muscle dystrophin expression, a finding consistent with our previous results following intramuscular injection in this muscle;[6] in other muscles slight but not significant

**Figure 5. Early systemic delivery of scAAV9.U7.ACCA in neonatal Dup2 mice drives long-lasting exon 2 skipping and dystrophin expression**

(A) RT-PCR quantification of tibialis anterior (TA), gastrocnemius (Gas), triceps (Tri), heart, and diaphragm (Dia) RNA from young Dup2 mice treated with $3.2 \times 10^{14}$ vg/kg scAAV9.U7.ACCA (ACCA) 1, 3, and 6 months post injection. Data are presented as mean ± SD (n = 4–9 per group). (B) Western blots of triceps dystrophin in young ACCA-treated Dup2 mice. The standard curve on the right shows incremental dilutions of pooled Bl6 samples in dystrophin-null muscle lysate. (C) Quantification of western blots shown in (B), presented as mean ± SD with individual points. The dashed line indicates 100% based on the standard curve. Dup2 Tri control group is reproduced from Figure 2B. (D) Representative images of dystrophin immunofluorescence (IF) in heart and triceps sections, and quantification of fiber dystrophin positivity in triceps. Images were processed identically with shading correction, rolling-ball background subtraction, and denoising (see Figure S9 for unprocessed images). Color-coded heatmaps reflect the percent dystrophin-positive perimeter for each muscle fiber, as indicated by the color scale. Fibers that have dystrophin around ≥30% of the perimeter are considered dystrophin positive. Scale bars, 200 μm. (E and F) Quantification of dystrophin IF intensity and percent dystrophin-positive fibers (PDPF) in muscle and heart sections, presented as mean ± SD with individual points. Untreated Dup2 and Bl6 groups show all tissues together. No statistically significant differences were identified between 3- and 6-month expression by unpaired t test (western blot) and two-way ANOVA (IF).

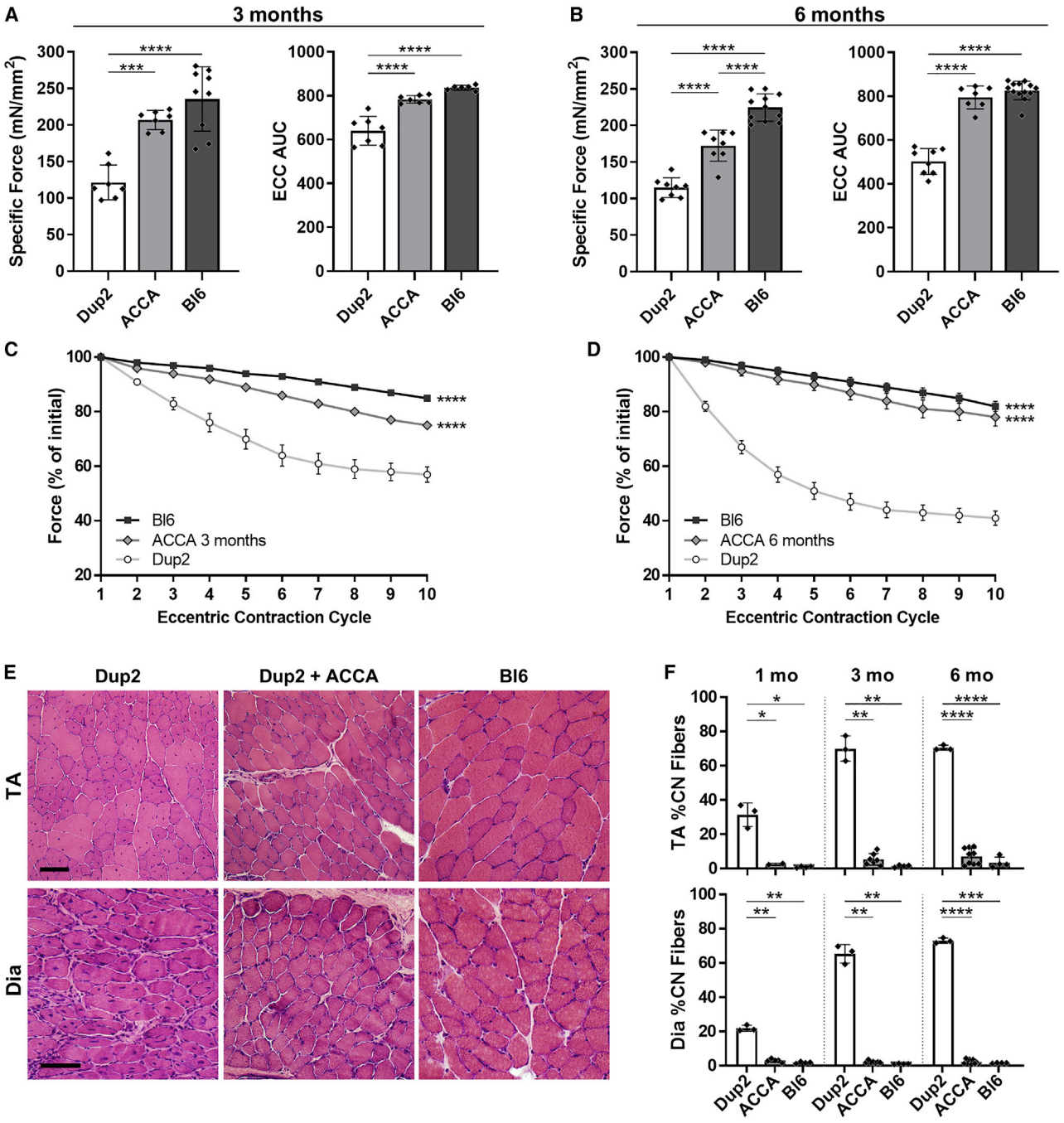


**Figure 6. Early systemic delivery of scAAV9.U7.ACCA in neonatal Dup2 mice prevents muscle pathology for at least 6 months**

All injections were performed in neonatal mice at P0–P1. (A and C) Specific force and force loss induced by eccentric contractions (ECC) in tibialis anterior (TA) muscles of 3-month-old Dup2 mice after ACCA treatment, compared with age-matched Bl6 and untreated Dup2 controls. ECC area under the curve (AUC) is calculated from force tracings over ten eccentric contraction cycles. (B and D) Specific force and ECC-induced force loss in TA muscles of 6-month-old Dup2 mice after ACCA treatment, compared with age-matched Bl6 and untreated Dup2 controls. (E) Representative H&E staining of TA and diaphragm (Dia) from treated Dup2 and control mice. Scale bars, 100 μm. (F) Quantification of centronucleation (CN) in myofibers from TA and Dia 1, 3, and 6 months after ACCA treatment. All bar graph data are presented as mean ± SD with individual points, and statistical comparisons were performed using one-way ANOVA with Sidak multiple comparisons test. ECC cycle tracings show mean ± SEM and were compared using two-way ANOVA with Bonferroni multiple comparisons test. *$p < 0.01$; **$p < 0.05$; ***$p < 0.001$; ****$p < 0.0001$ versus Dup2.

improvements of dystrophin expression were seen with PDN treatment. The reason for this discrepancy is not clear, although the overall responsiveness of the IRES element may improve dystrophin expression in boys with DMD who are routinely treated with prednisone. This clinical prediction is supported by an observational study of a relatively large cohort of DMD patients who carry the Dup2 mutation, in which those patients treated with corticosteroids walked significantly longer than non-Dup2 genotype controls.[41]

We noted no evidence of toxicity in our study, consistent with our previous studies assessing safety at shorter periods post injection.[27,28] Analysis was performed in a blinded (albeit non-GLP-compliant) fashion; review by a pathologist of histological sections of the brain, gonads, kidney, lung, and spleen of treated and untreated Dup2 mice found no meaningful difference between both groups (Figure S12). Although some livers occasionally had patchy small foci of inflammation that may contain neutrophils, this non-specific finding has also been reported in other AAV programs. Overall these results support the tolerability of AAV9 treatment in mice but do not replace the rigorous GLP-compliant IND-enabling toxicity studies that lead to clinical trial.[28]

In this study, we did not differentiate the 427 kDa WT dystrophin versus the 413 kDa IRES-driven forms of dystrophin, as reproducible separation by western blot is problematic. Nevertheless, skipping of exon 2 results in expression of both isoforms and—as the patients expressing dystrophin from the c.9G>A allele demonstrate[23,24]—both are therapeutic. RT-PCR demonstrated that, on average, the Del2 transcript makes up 65% of total therapeutic transcripts after ACCA treatment and 75% after ACCA + PDN treatment in adult mice (Figure 1B), and 61% of total therapeutic transcripts in neonatally treated mice (Figure 5A), suggesting that most of the induced dystrophin expression is likely IRES driven. Notably, the presence of this isoform is able to protect muscle from contraction-induced injury and correct muscle force to near control levels, despite missing half of the canonical ABD1, as translation beginning in exon 6 results in a protein lacking the first of two calponin homology domains (CH1 and CH2). These results suggest the need for further characterization of domains thought necessary for proper dystrophin function, with a goal of raising therapeutic possibilities. For example, the removal of CH2 in GRMD apparently leads to a similarly highly functional protein,[20,21] suggesting the need for further characterization of dystrophin structure-function relationships.

Our results demonstrate the robustness, durability, and safety of exon 2 skipping following delivery of scAAV9.U7snRNA.ACCA, substantiating the evidence that supported moving to clinic trials. scAAV9.U7.ACCA could represent a potential therapy for around 1.1% of all DMD patients. Furthermore, if this AAV.U7 tool proves to be successful in humans, it is easy to imagine how it can be repurposed for various other hotspots of DMD such as exons 51, 53, 44, and 45 that do not encode for critical protein domains, such as other teams have done.[42] We demonstrate here not only a potential treatment for patients with a duplication of exon 2 but also provide support for the use of the AAV.U7 system as a treatment for many other DMD mutations and other neuromuscular disorders.

## MATERIALS AND METHODS

### Constructs

The mouse U7 snRNA gene and smOPT sequences were cloned as U7-ACCA containing two U7snRNA antisense masking the acceptor site and two masking the splice donor site.[6,43] These were cloned in tandem in a self-complementary AAV vector. All plasmid constructs were sequence verified. Both inverted terminal repeat and self-complementary AAV backbone were checked using SmaI and MscI, respectively.

### AAV production

scAAV9.U7.ACCA was produced at the NCH Viral Vector Core (VVC), via 3-plasmid DNA transfection of human HEK 293 VVC Master Cell Bank cells with (1) the pAAV.U7-ACCA vector plasmid, (2) an AAV9 helper plasmid containing the AAV rep2 and cap9 WT genes, and (3) the helper adenovirus plasmid pHELP. Cells were cultivated in Corning Cell Stacks and lysed, using methodology standard to the NCH VVC. Two days post transfection, both cells and media were collected.

### Study design

All experimental procedures involving animals in this study were reviewed and approved by the Institutional Animal Care and Use Committee at Nationwide Children's Hospital. Because DMD almost exclusively affects males, only male mice were used in this study. Mice were housed in a barrier facility with HEPA-filtered air that is AAALAC accredited, and maintained with a 12/12-h light/dark cycle. Animals were clustered by groups; no randomization was used. AAV injections were conducted in a nonblinded fashion, but all dissection and most experiments were performed in a blinded fashion. The sample sizes were determined on the basis of previous experience, and supplementary tables and graphs with individual scatter points reflect the number of animals used for each experiment. No statistical methods were used to predetermine sample size prior to experimentation.

### Glucocorticoid treatment

6α-Methylprednisolone 21-hemisuccinate sodium salt (PDN; M3781, Sigma) was administered by intraperitoneal injection (12 mg/kg per day) for 3 weeks, five times per week. Control animals received phosphate buffered saline (PBS).

### Tail vein injection

Injection was performed in 2-month-old mice using a tail vein apparatus. The tail was warmed by a light bulb to enlarge the veins; once visible, AAV9 or PBS was injected with 300 μL corresponding to $1.9 \times 10^{12}$ vg ($7.6 \times 10^{13}$ vg/kg; maximum dose/volume possible to inject at that time point) of scAAV9.U7.ACCA in 300 μL total of PBS, or PBS alone, using a 33-gauge gas-tight Hamilton syringe. Following injection, a sterile cotton pad was placed on the injection site and held with pressure until bleeding ceased.

### Facial vein injection

Newborn pups (P0–P1) were anesthetized via placement on ice. Anesthetized pups were placed on a clean surface and held steady between the thumb and index finger, and an insulin needle was inserted into the cranial vein about 1 mm above the eye (either side) and 0.5–1 mm deep. Mice were injected with 50 μL corresponding to $3.2 \times 10^{11}$ vg ($3.2 \times 10^{14}$ vg/kg; maximum dose/volume possible to inject at that time point) of scAAV9.U7.ACCA in 50 μL total of PBS, or PBS alone, using a 33-gauge gas-tight Hamilton syringe. Following the injection, pups were placed on a heating pad to recover.

### Muscle preparation

Mouse necropsy was performed using standard techniques. Muscles were collected and either snap frozen in liquid nitrogen or mounted in tragacanth gum and frozen in liquid nitrogen-cooled isopentane for cryosectioning. Muscle sections were cut at 10 μm for immunofluorescence and H&E staining. Tissues/organs for histopathology studies were collected and fixed in 10% neutral buffered formalin (NBF).

### Quantitative PCR

Vector genomes were quantified in cardiac and skeletal muscles (TA, triceps brachii, gastrocnemius, and diaphragm). Total DNA was extracted from tissue samples using DNeasy Blood & Tissue Kit (catalog #69506; Qiagen, Germantown, MD, USA), and vector genomes quantified by qPCR using a linearized AAV.U7.ACCA plasmid to generate a standard curve allowing absolute quantification. The DNA samples were analyzed using TaqMan Universal PCR Master Mix (catalog #4304437; Applied Biosystems, Foster City, CA USA) and Quantstudio6 Flex (Applied Biosystems) following the procedures recommended by the manufacturer, and a set of primers unique to the transgene (sequences available upon request). Genomic DNA from non-injected and PDN-injected mouse tissues served as experimental control samples. Each sample was run in triplicate. Acceptance criteria for an assay included a standard curve with an R2 of 0.9900 or greater, efficiency between 90% and 110%, or a slope between 3.1 and 3.5, and undetermined values in the non-template control reactions.

### Reverse transcription, PCR amplification, and quantification

Reverse transcription (RT) was performed according to the manufacturer (Maxima reverse transcriptase, Ferk1672, or RevertAid First Strand cDNA Synthesis Kit, K1621; Thermo Fisher Scientific) using 1 μg of RNA and a mixture of random hexamer and oligo(dT) for each RT reaction. PCR amplification was performed using 2× Master Mix (K0172; Thermo Scientific) and 150 ng of RT product as template. Several pairs of primers were used for this study, and sequences are available upon request. Following electrophoresis, quantification of Dup2, WT, or Del2 transcript was performed using ImageJ, and each band was plotted in GraphPad Prism (version 9.0) as a percentage of the overall dystrophin transcript.

### Protein extraction and western blotting

Mouse muscle lysates were prepared using 4 M urea lysis buffer (pH 6.8); 150 μL of lysis buffer was added to ten sections of 20-μm-thick tissue. Tissue was lysed using a metal bead (2 min at 30 Hz, TissueLyser II; Qiagen). The solution was incubated at room temperature for 30 min prior to a second lysis step (1 min at 30 Hz, TissueLyser II). The solution was incubated again at room temperature for 30 min. The solution was then centrifuged at 14,000 × *g* for 20 min and supernatant extracted for analysis. Protein was quantified using a Bio-Rad DC assay kit (catalog #5000112). A calibration curve was made by spiking in WT dystrophin from C57Bl/6 mice into dystrophin-null lysate from a Dup2Del18-41 mouse. All samples were mixed with 4× Laemmli buffer prior to incubation at 95°C for 5 min. Thirty micrograms of total protein was loaded on a precast 3%–8% tri-acetate gel and ran for 1 h at 80 V followed by 2 h at 120 V. Gels were transferred overnight at 4°C, constant 55 mA onto a 0.45-μm polyvinylidene fluoride membrane. Membranes were cut at 150 kDa marker for probing. The top halves of membranes were probed using a polyclonal rabbit antibody specific to the C terminus of dystrophin (ab15277, 1:200 or ab154168, 1:1,000; Abcam). Membranes were then washed four times for 5 min in 0.1% Tween 20 containing PBS (PBST). Secondary antibody goat anti-rabbit HRP (1:5,000) for 1 h at room temperature followed by five 5-min washes with PBST and one 5-min wash with PBS. Membranes were incubated with 2 mL of ECL reagent (Thermo Scientific, #34580) prior to visualization on a Chemidoc MP Imaging System. Dystrophin signals were quantified using Image Lab software (version 6.0.0 build 25). Individual mouse samples were quantified using a linear regression curve fitted to a calibration curve on each gel. The full-length (427 kDa) and IRES-driven (413 kDa) dystrophin isoforms could not be differentiated on the western blots.

### Immunohistochemistry

Sections (10 μm thick) of cryopreserved tissues were air-dried for 30 min before staining. Following rehydration in PBS, sections were permeabilized using permeabilization solution (2% normal goat serum [NGS] + 0.1% Triton X-100 in PBS) for 10 min at room temperature. Sections were then incubated for 1 h with blocking solution (15% NGS in PBS) followed by a 2-h incubation with an anti-mouse immunoglobulin G unconjugated Fab fragment at room temperature. Primary antibodies (diluted in PBS +2% NGS) were incubated 2h or overnight at 4°C. Sections were then washed four times for 5 min with 1× PBS at room temperature. Secondary dye-conjugated antibodies diluted in PBS + 2% NGS were added to muscle sections for 1 h at room temperature. Following three washes, DAPI solution was added to stain the nucleus. Sections were then mounted using PVA-DABCO. The following primary antibodies were used: dystrophin (1:400; ab15277, Abcam); α1-laminin (1:400; MAB4656, R&D Systems); nNos (1:200; sc-648, SCBT); β-dystroglycan (1:500; MANDAG2, DSHB or gift from Dr. Glenn Morris and the MDA Monoclonal Antibody Resource, www.glennmorris.org.uk); β-sarcoglycan (1:50; B-SARC-L-CE, Novocastra). Secondary antibodies conjugated to Alexa Fluor were used at 1:500 dilution.

Images of representative tissue regions were captured on an Olympus Bx61 motorized epifluorescence microscope with a DP71 camera with a 0.5× relay lens and a UPlanSApo 10× objective at a resolution of

1.29 μm/pixel. Several images were taken for each muscle (representative images are shown in the figures).

#### Dystrophin immunofluorescence analysis

Automated image processing and analysis of dystrophin-positive fibers and dystrophin intensity was performed with Nikon NIS-Elements AR software on multichannel images of dystrophin and laminin immunofluorescence using methods described previously.[26] Only images that were captured within the same batch and under the same exposure settings were quantified together as a set, and images reflecting unacceptable tissue quality or staining were excluded from quantification. In preparation for analysis, all images were preprocessed in an automated and identical fashion using shading correction, rolling-ball background subtraction, and denoising to reduce the impact of uneven background signal and illumination.

In brief, all muscle fibers were identified based on laminin staining by the artificial intelligence (AI) software module Segment.ai, which was originally trained as previously described and deployed on this image set without further training.[26] Satisfactory AI performance was confirmed before proceeding with the analysis. Following AI-based segmentation of muscle fibers, dystrophin-positive and laminin-positive pixels were automatically identified around each muscle fiber using automatic thresholds derived from signal intensities within the images. Dystrophin positivity was then calculated by measuring the combined length of dystrophin-positive segments around each muscle fiber perimeter and normalizing it to the length of the laminin-positive perimeter. A color-coded overlay image of all muscle fiber perimeter regions and their positivity was automatically produced as an output of the analysis. Consistently with our prior work,[26,29] a muscle fiber was considered overall positive for dystrophin if 30% or more of the perimeter had a dystrophin-positive signal.

Dystrophin signal intensity was measured in skeletal muscles and hearts under a laminin-positive image mask and was normalized to the laminin intensity of the same pixels for each image. The laminin-positive pixel mask was identified using an automatic multilevel Otsu threshold, and the mean intensity of all image pixels under the mask was measured in both channels.

#### Centronucleation analysis

H&E staining was performed using the standard technique, and fiber counting was performed manually using ImageJ. Three sections were processed and counted for each animal. Analysis of the data was performed blindly but not randomly.

#### Force generation and protection from eccentric contractions

Force assessment in the TA was performed using standard techniques[44] modified as described elsewhere.[6] Specific force was obtained by dividing the maximum tetanic force by the TA muscle cross-sectional area. After the eccentric contractions, the mice were euthanized and the TA muscle was dissected out, weighed, and frozen for analysis. Analysis of the data was performed blindly but not randomly.

#### Statistical analysis

Statistical analyses were performed using GraphPad Prism (version 9.0). Experiments involving two independent variables (tissue and treatment, time and treatment, or tissue and time) were analyzed using two-way ANOVA with the Sidak multiple comparisons test for individual pairwise comparisons. Experiments with a single independent variable were analyzed using one-way ANOVA with the Sidak multiple comparisons test, or unpaired t test if involving only one comparison. Eccentric contraction-induced force loss was analyzed over ten contraction cycles using two-way ANOVA with the Bonferroni multiple comparisons test. All statistical methods are identified in the legends for the corresponding figures and supplementary tables for each assay.

#### RNA and RPF isolation and sequencing

Frozen TA muscle from control and scAAV9.U7.ACCA treated Dup2 mice were sectioned on a cryostat and homogenized with a 26-gauge needle in 400 mL of 20 mM Tris-HCl (pH 7.4), 150 mM NaCl, 5 mM $MgCl_2$, 1 mM dithiothreitol, 1% Triton X-100, and 100 μg/mL cycloheximide. Ribosome-protected fragments were isolated from one-half of the homogenate as previously described.[6] Total RNA was extracted from the other half using TRIzol (Invitrogen, #15596018) and precipitated with isopropanol according to the manufacturer's instructions (Life Technologies), and rRNA was depleted using Ribo-Zero rRNA Removal Kit Human/Mouse/Rat (Epicentre). Illumina TruSeq Stranded Total RNA library kits were used to prepare indexed libraries, and 50 bp reads were generated on an Illumina HiSeq instrument using v4 chemistry. RPF-seq libraries were prepared using the Illumina TruSeq Small RNA Sample Kit according to the manufacturer's specifications, and 50 bp reads were generated on an Illumina HiSeq instrument. Trimmed and filtered RPF-seq and RNA-seq reads were mapped to reference genomes using the STAR aligner or to transcript sequences using cross_match. Perl scripts were used to generate read count tables from mapped RPF-seq and RNA-seq reads, and *edgeR* (Bioconductor) was used for model-based read count normalization. The RPF-seq and RNA-seq data have been deposited in NCBI's Gene Expression Omnibus and are accessible through series accession number GEO: GSE195480.

#### Organ pathology assessment

Following fixation in 10% NBF, all non-skeletal-muscle tissues were embedded in paraffin and sectioned at 12 μm or less, stained with H&E, and microscopically examined for histopathology by Dr. C. Pierson, a board-certified anatomic pathologist and neuropathologist. Analysis of the data was performed blindly but not randomly.

## DATA AVAILABILITY

Data supporting the studies presented in this paper can be made available by request to the corresponding authors.

## SUPPLEMENTAL INFORMATION

Supplemental information can be found online at https://doi.org/10.1016/j.omtm.2022.07.005.

## ACKNOWLEDGMENTS

The authors wish to acknowledge Kara Flint, Jacob Lay, Felecia Gumienny, Jacqueline Yurkoski, and Diane Dunn for technical assistance, and Kristen Heller and Louise Rodino-Klapac for helpful discussions. Chris Pierson performed the analysis of histopathology. This work occurred under appropriate instiutional approvals for animal studies including IACUC#: AR10-00002, AR11-00032, and IBCSC#: IBS00000123. This work was supported in part by a grant awards to K.M.F. from the Association Française contre les Myopathies and by CureDuchenne.

## AUTHOR CONTRIBUTIONS

N.W. and N.H. administered the injections of scAAV9.U7.ACCA and performed immunostaining on mouse muscle, and performed RT-PCR with contributions from D.L. and D.R. A.V. generated the Dup2 mouse model. T.R.S. and L.V.G. performed or analyzed the muscle-specific force and ECC tests. T.A.V. developed and performed the IF blinded analysis. E.C.F. and C.F.A. performed the qPCR, and E.C.F. completed RT-PCR analysis. A.B. performed the western blots. R.B.W. designed and performed the ribosome profiling experiments. N.W., A.V., T.R.S., T.A.V., and K.M.F. designed the experiments, and analyzed and interpreted the data. N.W., R.B.W., T.A.V., and K.M.F. wrote the manuscript and compiled the figures, with contributions from A.V. and T.R.S.

## DECLARATION OF INTERESTS

Since the performance of this work, Nationwide Children's Hospital licensed the vector described herein to Audentes/Astellas Therapeutics. N.W., A.V., and K.M.F. have received royalty payments as a result of this license.

## REFERENCES

1. Mendell, J.R., Shilling, C., Leslie, N.D., Flanigan, K.M., al-Dahhak, R., Gastier-Foster, J., Kneile, K., Dunn, D.M., Duval, B., Aoyagi, A., et al. (2012). Evidence-based path to newborn screening for Duchenne muscular dystrophy. Ann. Neurol. *71*, 304–313. https://doi.org/10.1002/ana.23528.

2. Passamano, L., Taglia, A., Palladino, A., Viggiano, E., D'Ambrosio, P., Scutifero, M., Rosaria Cecio, M., Torre, V., Luca, F.D.E., Picillo, E., et al. (2012). Improvement of survival in Duchenne Muscular Dystrophy: retrospective analysis of 835 patients. Acta Myol. *31*, 121–125.

3. Duchenne. (1867). The pathology of paralysis with muscular degeneration (paralysie myosclerotique), or paralysis with apparent hypertrophy. Br. Med. J. *2*, 541–542. https://doi.org/10.1136/bmj.2.363.541.

4. Juan-Mateu, J., Gonzalez-Quereda, L., Rodriguez, M.J., Baena, M., Verdura, E., Nascimento, A., Ortez, C., Baiget, M., and Gallano, P. (2015). DMD mutations in 576 dystrophinopathy families: a step forward in genotype-phenotype correlations. PLoS One *10*, e0135189. https://doi.org/10.1371/journal.pone.0135189.

5. Petrof, B.J., Shrager, J.B., Stedman, H.H., Kelly, A.M., and Sweeney, H.L. (1993). Dystrophin protects the sarcolemma from stresses developed during muscle contraction. Proc. Natl. Acad. Sci. USA *90*, 3710–3714. https://doi.org/10.1073/pnas.90.8.3710.

6. Wein, N., Vulin, A., Falzarano, M.S., Szigyarto, C.A., Maiti, B., Findlay, A., Heller, K.N., Uhlen, M., Bakthavachalu, B., Messina, S., et al. (2014). Translation from a DMD exon 5 IRES results in a functional dystrophin isoform that attenuates dystrophinopathy in humans and mice. Nat. Med. *20*, 992–1000. https://doi.org/10.1038/nm.3628.

7. Monaco, A.P. (1989). Dystrophin, the protein product of the Duchenne/Becker muscular dystrophy gene. Trends Biochem. Sci. *14*, 412–415. https://doi.org/10.1016/0968-0004(89)90290-9.

8. Muzyczka, N. (1992). Use of adeno-associated virus as a general transduction vector for mammalian cells. Curr. Top. Microbiol. Immunol. *158*, 97–129. https://doi.org/10.1007/978-3-642-75608-5_5.

9. Carter, B.J. (2004). Adeno-associated virus and the development of adeno-associated virus vectors: a historical perspective. Mol. Ther. *10*, 981–989. https://doi.org/10.1016/j.ymthe.2004.09.011.

10. Samulski, R.J., and Muzyczka, N. (2014). AAV-mediated gene therapy for research and therapeutic purposes. Annu. Rev. Virol. *1*, 427–451. https://doi.org/10.1146/annurev-virology-031413-085355.

11. Duan, D. (2018). Systemic AAV micro-dystrophin gene therapy for duchenne muscular dystrophy. Mol. Ther. *26*, 2337–2356. https://doi.org/10.1016/j.ymthe.2018.07.011.

12. Harper, S.Q., Hauser, M.A., DelloRusso, C., Duan, D., Crawford, R.W., Phelps, S.F., Harper, H.A., Robinson, A.S., Engelhardt, J.F., Brooks, S.V., and Chamberlain, J.S. (2002). Modular flexibility of dystrophin: implications for gene therapy of Duchenne muscular dystrophy. Nat. Med. *8*, 253–261. https://doi.org/10.1038/nm0302-253.

13. Barthelemy, F., and Wein, N. (2018). Personalized gene and cell therapy for duchenne muscular dystrophy. Neuromuscul. Disord. *28*, 803–824. https://doi.org/10.1016/j.nmd.2018.06.009.

14. Wein, N., Alfano, L., and Flanigan, K.M. (2015). Genetics and emerging treatments for Duchenne and Becker muscular dystrophy. Pediatr. Clin. North. Am *62*, 723–742. https://doi.org/10.1016/j.pcl.2015.03.008.

15. Alfano, L.N., Charleston, J.S., Connolly, A.M., Cripe, L., Donoghue, C., Dracker, R., Dworzak, J., Eliopoulos, H., Frank, D.E., Lewis, S., et al. (2019). Long-term treatment with eteplirsen in nonambulatory patients with Duchenne muscular dystrophy. Medicine (Baltim.) *98*, e15858. https://doi.org/10.1097/MD.0000000000015858.

16. Gorman, L., Suter, D., Emerick, V., Schumperli, D., and Kole, R. (1998). Stable alteration of pre-mRNA splicing patterns by modified U7 small nuclear RNAs. Proc. Natl. Acad. Sci. USA *95*, 4929–4934. https://doi.org/10.1073/pnas.95.9.4929.

17. Suter, D., Tomasini, R., Reber, U., Gorman, L., Kole, R., and Schumperli, D. (1999). Double-target antisense U7 snRNAs promote efficient skipping of an aberrant exon in three human beta-thalassemic mutations. Hum. Mol. Genet. *8*, 2415–2423. https://doi.org/10.1093/hmg/8.13.2415.

18. Goyenvalle, A., Babbs, A., Wright, J., Wilkins, V., Powell, D., Garcia, L., and Davies, K.E. (2012). Rescue of severely affected dystrophin/utrophin-deficient mice through scAAV-U7snRNA-mediated exon skipping. Hum. Mol. Genet. *21*, 2559–2571. https://doi.org/10.1093/hmg/dds082.

19. Barbash, I.M., Cecchini, S., Faranesh, A.Z., Virag, T., Li, L., Yang, Y., Hoyt, R.F., Kornegay, J.N., Bogan, J.R., Garcia, L., et al. (2013). MRI roadmap-guided transendocardial delivery of exon-skipping recombinant adeno-associated virus restores dystrophin expression in a canine model of Duchenne muscular dystrophy. Gene Ther. *20*, 274–282. https://doi.org/10.1038/gt.2012.38.

20. Bish, L.T., Sleeper, M.M., Forbes, S.C., Wang, B., Reynolds, C., Singletary, G.E., Trafny, D., Morine, K.J., Sanmiguel, J., Cecchini, S., et al. (2012). Long-term restoration of cardiac dystrophin expression in golden retriever muscular dystrophy following rAAV6-mediated exon skipping. Mol. Ther. *20*, 580–589. https://doi.org/10.1038/mt.2011.264.

21. Vulin, A., Barthelemy, I., Goyenvalle, A., Thibaud, J.L., Beley, C., Griffith, G., Benchaouir, R., le Hir, M., Unterfinger, Y., Lorain, S., et al. (2012). Muscle function recovery in golden retriever muscular dystrophy after AAV1-U7 exon skipping. Mol. Ther. *20*, 2120–2133. https://doi.org/10.1038/mt.2012.181.

22. Bladen, C.L., Salgado, D., Monges, S., Foncuberta, M.E., Kekou, K., Kosma, K., Dawkins, H., Lamont, L., Roy, A.J., Chamova, T., et al. (2015). The TREAT-NMD DMD Global Database: analysis of more than 7,000 Duchenne muscular dystrophy mutations. Hum. Mutat. *36*, 395–402. https://doi.org/10.1002/humu.22758.

23. Flanigan, K.M., Dunn, D.M., von Niederhausern, A., Howard, M.T., Mendell, J., Connolly, A., Saunders, C., Modrcin, A., Dasouki, M., Comi, G.P., et al. (2009). DMD Trp3X nonsense mutation associated with a founder effect in North

American families with mild Becker muscular dystrophy. Neuromuscul. Disord. *19*, 743–748. https://doi.org/10.1016/j.nmd.2009.08.010.

24. Gurvich, O.L., Maiti, B., Weiss, R.B., Aggarwal, G., Howard, M.T., and Flanigan, K.M. (2009). DMD exon 1 truncating point mutations: amelioration of phenotype by alternative translation initiation in exon 6. Hum. Mutat. *30*, 633–640. https://doi.org/10.1002/humu.20913.

25. Vulin, A., Wein, N., Simmons, T.R., Rutherford, A.M., Findlay, A.R., Yurkoski, J.A., Kaminoh, Y., and Flanigan, K.M. (2015). The first exon duplication mouse model of Duchenne muscular dystrophy: a tool for therapeutic development. Neuromuscul. Disord. *25*, 827–834. https://doi.org/10.1016/j.nmd.2015.08.005.

26. Simmons, T.R., Vetter, T.A., Huang, N., Vulin-Chaffiol, A., Wein, N., and Flanigan, K.M. (2021). Pre-clinical dose-escalation studies establish a therapeutic range for U7snRNA-mediated DMD exon 2 skipping. Mol. Ther. Methods Clin. Dev. *21*, 325–340. https://doi.org/10.1016/j.omtm.2021.03.014.

27. Wein, N., Dunn, D.M., Waldrop, M.A., Gushchina, L.V., Frair, E.C., Weiss, R.B., and Flanigan, K.M. (2021). Absence of significant off-target splicing variation with a U7snRNA vector targeting DMD exon 2 duplications. Hum. Gene Ther. *32*, 1346–1359. https://doi.org/10.1089/hum.2020.315.

28. Gushchina, L.V., Frair, E.C., Rohan, N., Bradley, A.J., Simmons, T.R., Chavan, H.D., Chou, H.J., Eggers, M., Waldrop, M.A., Wein, N., and Flanigan, K.M. (2021). Lack of toxicity in nonhuman primates receiving clinically relevant doses of an AAV9.U7snRNA vector designed to induce DMD exon 2 skipping. Hum. Gene Ther. *32*, 882–894. https://doi.org/10.1089/hum.2020.286.

29. Vetter, T.A., Nicolau, S., Bradley, A.J., Frair, E.C., and Flanigan, K.M. (2021). Automated immunofluorescence analysis for sensitive and precise dystrophin quantification in muscle biopsies. Neuropathol. Appl. Neurobiol. https://doi.org/10.1111/nan.12785.

30. Chang, W.J., Iannaccone, S.T., Lau, K.S., Masters, B.S., McCabe, T.J., McMillan, K., Padre, R.C., Spencer, M.J., Tidball, J.G., and Stull, J.T. (1996). Neuronal nitric oxide synthase and dystrophin-deficient muscular dystrophy. Proc. Natl. Acad. Sci. USA *93*, 9142–9147. https://doi.org/10.1073/pnas.93.17.9142.

31. Haslett, J.N., Sanoudou, D., Kho, A.T., Bennett, R.R., Greenberg, S.A., Kohane, I.S., Beggs, A.H., and Kunkel, L.M. (2002). Gene expression comparison of biopsies from Duchenne muscular dystrophy (DMD) and normal skeletal muscle. Proc. Natl. Acad. Sci. USA *99*, 15000–15005. https://doi.org/10.1073/pnas.192571199.

32. Clemens, P.R., Rao, V.K., Connolly, A.M., Harper, A.D., Mah, J.K., Smith, E.C., McDonald, C.M., Zaidman, C.M., Morgenroth, L.P., Osaki, H., et al. (2020). Safety, tolerability, and efficacy of viltolarsen in boys with duchenne muscular dystrophy amenable to exon 53 skipping: a phase 2 randomized clinical trial. JAMA Neurol. *77*, 982–991. https://doi.org/10.1001/jamaneurol.2020.1264.

33. Frank, D.E., Schnell, F.J., Akana, C., El-Husayni, S.H., Desjardins, C.A., Morgan, J., Charleston, J.S., Sardone, V., Domingos, J., Dickson, G., et al. (2020). Increased dystrophin production with golodirsen in patients with Duchenne muscular dystrophy. Neurology *94*, e2270–e2282. https://doi.org/10.1212/WNL.0000000000009233.

34. Charleston, J.S., Schnell, F.J., Dworzak, J., Donoghue, C., Lewis, S., Chen, L., Young, G.D., Milici, A.J., Voss, J., DeAlwis, U., et al. (2018). Eteplirsen treatment for Duchenne muscular dystrophy: exon skipping and dystrophin production. Neurology *90*, e2146–e2154. https://doi.org/10.1212/WNL.0000000000005680.

35. Alter, J., Lou, F., Rabinowitz, A., Yin, H., Rosenfeld, J., Wilton, S.D., Partridge, T.A., and Lu, Q.L. (2006). Systemic delivery of morpholino oligonucleotide restores dystrophin expression bodywide and improves dystrophic pathology. Nat. Med. *12*, 175–177. https://doi.org/10.1038/nm1345.

36. Yokota, T., Lu, Q.L., Partridge, T., Kobayashi, M., Nakamura, A., Takeda, S., and Hoffman, E. (2009). Efficacy of systemic morpholino exon-skipping in Duchenne dystrophy dogs. Ann. Neurol. *65*, 667–676. https://doi.org/10.1002/ana.21627.

37. Kornegay, J.N. (2017). The golden retriever model of Duchenne muscular dystrophy. Skelet Muscle *7*, 9. https://doi.org/10.1186/s13395-017-0124-z.

38. Le Hir, M., Goyenvalle, A., Peccate, C., Precigout, G., Davies, K.E., Voit, T., Garcia, L., and Lorain, S. (2013). AAV genome loss from dystrophic mouse muscles during AAV-U7 snRNA-mediated exon-skipping therapy. Mol. Ther. *21*, 1551–1558. https://doi.org/10.1038/mt.2013.121.

39. Aartsma-Rus, A., Morgan, J., Lonkar, P., Neubert, H., Owens, J., Binks, M., Montolio, M., Phadke, R., Datson, N., Van Deutekom, J., et al. (2019). Report of a TREAT-NMD/world duchenne organisation meeting on dystrophin quantification methodology. J. Neuromuscul. Dis. *6*, 147–159. https://doi.org/10.3233/JND-180357.

40. Waldrop, M.A., Gumienny, F., El Husayni, S., Frank, D.E., Weiss, R.B., and Flanigan, K.M. (2018). Low-level dystrophin expression attenuating the dystrophinopathy phenotype. Neuromuscul. Disord. *28*, 116–121. https://doi.org/10.1016/j.nmd.2017.11.007.

41. Zambon, A.A., Waldrop, M.A., Alles, R., Weiss, R.B., Conroy, S., Moore-Clingenpeel, M., Previtali, S., Flanigan, K.M., Italian, D.M.D.N., and the United Dystrophinopathy, P. (2021). Phenotypic spectrum of dystrophinopathy due to duchenne muscular dystrophy exon 2 duplications. Neurology. https://doi.org/10.1212/WNL.0000000000013246.

42. Domenger, C., Allais, M., Francois, V., Leger, A., Lecomte, E., Montus, M., Servais, L., Voit, T., Moullier, P., Audic, Y., and Le Guiner, C. (2018). RNA-seq analysis of an antisense sequence optimized for exon skipping in duchenne patients reveals No off-target effect. Mol. Ther. Nucleic Acids *10*, 277–291. https://doi.org/10.1016/j.omtn.2017.12.008.

43. Goyenvalle, A., Vulin, A., Fougerousse, F., Leturcq, F., Kaplan, J.C., Garcia, L., and Danos, O. (2004). Rescue of dystrophic muscle through U7 snRNA-mediated exon skipping. Science *306*, 1796–1799. https://doi.org/10.1126/science.1104297.

44. Hakim, C.H., Li, D., and Duan, D. (2011). Monitoring murine skeletal muscle function for muscle gene therapy. Methods Mol. Biol. *709*, 75–89. https://doi.org/10.1007/978-1-61737-982-6_5.